

# Conductance Fluctuations and Partially Broken Spin Symmetries in Quantum Dots

D. M. Zumbühl, J. B. Miller, and C. M. Marcus

*Department of Physics, Harvard University, Cambridge, Massachusetts 02138*

D. Goldhaber-Gordon

*Department of Physics, Stanford University, Stanford, California 94305*

J. S. Harris, Jr.

*Department of Electrical Engineering, Stanford University, Stanford, California 94305*

K. Campman and A. C. Gossard

*Materials Department, University of California, Santa Barbara, California 93106*

Conductance fluctuations in GaAs quantum dots with spin-orbit and Zeeman coupling are investigated experimentally and compared to a random matrix theory formulation that defines a number of regimes of spin symmetry depending on experimental parameters. Accounting for orbital coupling of the in-plane magnetic field, which can break time-reversal symmetry, yields excellent overall agreement between experiment and theory.

PACS numbers: 73.23.Hk, 73.20.Fz, 73.50.Gr, 73.23.-b

The combination of confinement, spin-orbit (SO) coupling, and Zeeman splitting in semiconductor quantum dots gives rise to rich physics, including experimental access to interesting partially-broken spin symmetries [1] and a suppression of SO effects due to confinement [1, 2, 3, 4, 5] that provides long spin lifetimes in small quantum dots [5, 6]. Further consequences of these combined effects are that the confinement-induced suppression of SO effects is lifted by adding a Zeeman field [1, 2, 3] or by allowing spatial dependence of the SO coupling [7]. Because of the finite thickness of a two-dimensional electron gas, an in-plane magnetic field  $B_{\parallel}$  will have an orbital coupling that affects the electron dispersion and can break time-reversal symmetry (TRS) [4, 8, 9, 10, 11, 12], adding additional complexity to this system.

This Letter presents an experimental study of mesoscopic conductance fluctuations in quantum dots that possess both significant SO and Zeeman coupling. We find that the  $B_{\parallel}$  dependence of the variance of conductance fluctuations,  $\text{var } g$ , with TRS explicitly broken by a perpendicular field ( $B_{\perp} \neq 0$ , i. e.,  $B_{\perp} \gg (h/e)/A$ , where  $A$  is the dot area) depends critically on the strength of SO coupling and dot size. This dependence can be understood in terms of spin symmetries partially broken by  $B_{\parallel}$  and is in quantitative agreement with an appropriate random matrix theory (RMT) formulation [1]. We also find that  $\text{var } g(B_{\perp}, B_{\parallel})$  becomes independent of  $B_{\perp}$  at large  $B_{\parallel}$  due to  $B_{\parallel}$  breaking TRS, consistent with previous results [4, 10]. Taking into account orbital coupling [8, 9], agreement between theory and experiment is excellent for both broken and unbroken TRS and various regimes of spin symmetry.

In quantum dots, effects of Rashba and linear Dresselhaus SO coupling are suppressed due to confinement in the absence of Zeeman coupling [1, 2, 5]. For large

Zeeman splitting or weak confinement, this suppression is lifted and new symmetry classes with partially broken spin symmetry appear. A random matrix theory (RMT) analysis of this system was developed by Aleiner *et al.* [1] and extended to include inhomogeneous SO coupling and interpolation between ensembles [1]. The RMT formulation identifies three symmetry parameters that govern the amplitude (variance) of conductance fluctuations,  $\text{var } g \propto s/(\beta\Sigma)$ . Here,  $\beta = \{1, 2, 4\}$  is the usual Dyson parameter reflecting TRS,  $s = \{1, 2\}$  accounts for Kramers degeneracy, and  $\Sigma = \{1, 2\}$  characterizes mixing between Kramers pairs. With these parameters, spin symmetry may be either unbroken ( $s = 2, \Sigma = 1$ ), partially broken ( $s = 1, \Sigma = 1$ ) or fully broken ( $s = 1, \Sigma = 2$ ), causing a reduction of the variance by a factor of two each time spin symmetry is incrementally broken. Temperature and decoherence also reduce  $\text{var}(g)$ , but ratios such as  $\text{var } g(B_{\parallel})/\text{var } g(B_{\parallel} = 0)$  are affected only weakly.

Conductance fluctuations are known to be reduced by SO and Zeeman coupling in bulk (disordered) mesoscopic samples, and theories [13, 14, 15] are in good agreement with experiments [16]. Recently, the combined effects of SO and Zeeman coupling on magneto resistance in bulk samples were investigated [11], reporting spin-induced breaking of TRS [12]. Experimental observation of partially broken spin symmetry, which has been theoretically predicted [1, 14], has to our knowledge not been previously reported. Results of Ref. [1] were used to explain existing data on  $\text{var } g(B_{\perp} \neq 0, B_{\parallel})$  [3] as well as subsequent experiments on average conductance (weak localization and antilocalization) in quantum dots [4, 17]. There have been no comparable studies of conductance fluctuations to investigate the various symmetry classes to our knowledge.

Four gate-defined quantum dots of various sizes on two heterostructure wafers were measured (see Table 1 and

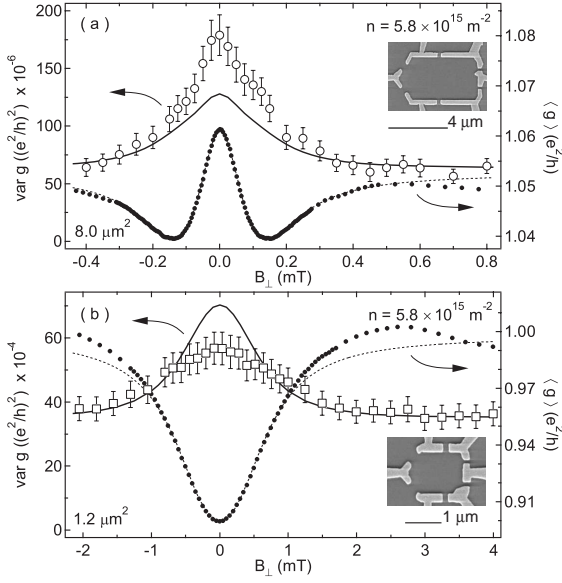


FIG. 1: Conductance average  $\langle g(B_{\perp}) \rangle$  (solid dots) and variance  $\text{var } g(B_{\perp})$  (open circles and squares) as a function of perpendicular magnetic field  $B_{\perp}$  with  $B_{\parallel} = 0$ , for large and small dots on the high density material, at  $T = 300$  mK. (a) Antilocalization in  $\langle g(B_{\perp}) \rangle$  for the  $8 \mu\text{m}^2$  dot. (b) Weak localization in  $\langle g(B_{\perp}) \rangle$  for the  $1.2 \mu\text{m}^2$  dot, demonstrating confinement suppression of SO effects. Both dots show an enhancement of  $\text{var } g$  at  $B_{\perp} = 0$ . Fits of RMT [1] to  $\langle g(B_{\perp}) \rangle$  (dashed curves) and  $\text{var } g(B_{\perp})$  (solid curves) using fit parameters determined from fits to  $\langle g \rangle$  plus an overall scale factor for  $\text{var } g$  (see text). Insets show device micrographs.

Figs. 1 and 2 insets). The lower density wafer showed weak localization at  $B_{\parallel} = 0$  [10], while the higher density material has sufficient SO coupling to exhibit antilocalization at  $B_{\parallel}$  [4]. Further details of these wafers are given in [4, 10]. Measurements were made in a  $^3\text{He}$  cryostat at  $0.3$  K using current bias of  $1$  nA at  $338$  Hz. In order to apply tesla-scale  $B_{\parallel}$  while maintaining sub-gauss control of  $B_{\perp}$ , we mount the sample with the 2DEG aligned to the axis of the primary solenoid (accurate to  $\sim 1^\circ$ ) and use an independent split-coil magnet attached to the cryostat to provide  $B_{\perp}$  [3]. The Hall voltage measured in a co-mounted Hall bar sample as well as the symmetry of transport through the dot itself (visible for  $B_{\parallel} \lesssim 2T$ ) was used to locate  $B_{\perp} = 0$  as it changed with  $B_{\parallel}$ .

Statistics of conductance fluctuations were gathered using two shape-distorting gates [18] while the point contacts were actively held at one fully transmitting mode each. At each value of  $B_{\perp}$  and  $B_{\parallel}$ , mean and variance were estimated based on  $\sim 400$  ( $\sim 200$ ) statistically independent samples for the low density (high density) dots. For  $\text{var } g(B_{\parallel}, B_{\perp} \neq 0)$  data with TRS explicitly broken,  $B_{\perp}$  was used to gather additional samples to reduced the statistical error.

Fitting the RMT results to  $\langle g(B_{\perp}) \rangle$  yields values for the average SO length  $\lambda_{so} = \sqrt{|\lambda_1 \lambda_2|}$ , where  $\lambda_{1,2}$  are the SO lengths along the main crystal axes, as well as the phase coherence time  $\tau_{\varphi}$  and a geometrical parameter  $\kappa_{\perp}$ . The SO inhomogeneity  $\nu_{so} = \sqrt{|\lambda_1 / \lambda_2|}$  can be

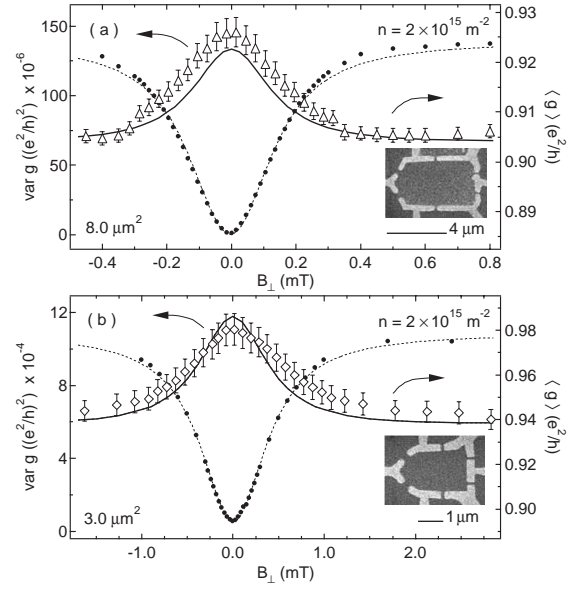


FIG. 2: Conductance average  $\langle g(B_{\perp}) \rangle$  (solid dots) and variance  $\text{var } g(B_{\perp})$  (open triangles and diamonds) as a function of perpendicular field  $B_{\perp}$  with  $B_{\parallel} = 0$ , for (a) large and (b) small dot, both fabricated on low density material. Both devices display weak localization in  $\langle g(B_{\perp}) \rangle$ . Fits to RMT is shown as dashed and solid curves, as described in the caption of Fig. 1. Insets show device micrographs; geometry of large device is identical to large dot in high density material.

extracted from  $\langle g(B_{\parallel}) \rangle$  in the presence of antilocalization (AL), and is taken as  $\nu_{so} = 1.4(1.0)$  for the high (low) density devices [4]. An additional order-one geometrical parameter  $\kappa'$ , relevant for the strong SO regime and not readily extracted from transport measurements, is set to  $\kappa' = 1$  for all devices. Further details of fits to the average conductance are given in Ref. [4]. We note that in absence of AL  $\lambda_{so}$  can only be bounded from below. Values for  $\tau_{\varphi}$  are similar for all devices and consistent with previous measurements [19].

As seen in Figs. 1 and 2, all devices except the large high density dot show weak localization (WL), indicating these dots are in the regime  $\lambda_{so} \gg L$ , where SO effects are strongly suppressed by confinement. The observation of WL down to  $\sim 40$  mK in previous measurements on identical devices [19] bounds the SO rate to  $\lambda_{so} \gtrsim 9 \mu\text{m}$ . We note that SO coupling of this order will noticeably re-

$n$ $\text{m}^{-2}$	$A$ $\mu\text{m}^2$	$\tau_{\varphi}$ ns	$\lambda_{so}$ $\mu\text{m}$	$\nu_{so}$	$\kappa_{\perp}$	$f_{var}$	$\xi$	a $\text{ns}^{-1}\text{T}^{-2}$	b $\text{ns}^{-1}\text{T}^{-6}$
2.0	3.0	0.18	8.5	1.0	0.15	1.0	2.8	$0.5 \pm 0.1$	0.028
2.0	8.0	0.21	8.5	1.0	0.25	0.6	3.0	$0.37 \pm 0.07$	0.028
5.8	1.2	0.10	3.2	1.4	0.33	1.9	1.0	$6.6 \pm 1$	0.14
5.8	8.0	0.39	4.4	1.4	0.23	0.7	0.45	$1.4 \pm 0.4$	0.14

TABLE I: Carrier density  $n$ , dot area  $A = L^2$ , coherence time  $\tau_{\varphi}$ , spin-orbit parameters  $\lambda_{so}$  and  $\nu_{so}$ , RMT parameters  $\kappa_{\perp}$ ,  $f_{var}$  and  $\xi$  and FJ parameters  $a$  and  $b$ , see text.

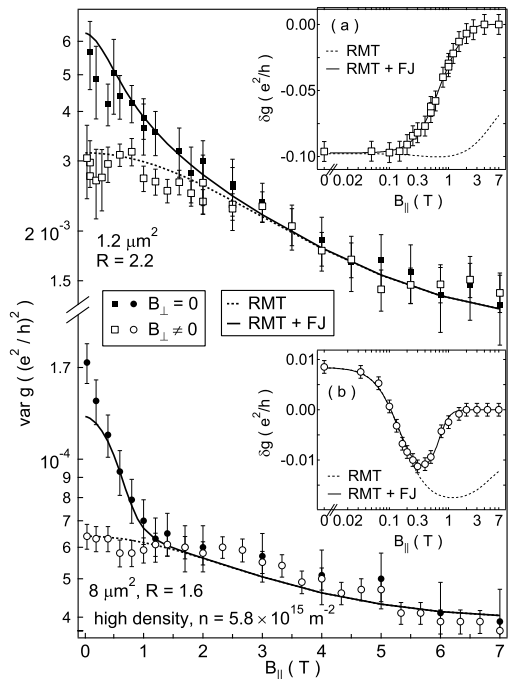


FIG. 3: Variance of conductance fluctuations,  $\text{var } g$ , in high density dots, as a function of in-plane field  $B_{\parallel}$  with  $B_{\perp} \neq 0$  sufficient to break TRS (open symbols) and  $B_{\perp} = 0$  (solid symbols). The big dot shows less reduction in  $\text{var } g(B_{\perp} \neq 0)$  with  $B_{\parallel}$  than the small dot, consistent with RMT, see text. Insets show quantum correction to average conductance,  $\delta g(B_{\parallel}) = \langle g(B_{\perp} = 0, B_{\parallel}) \rangle - \langle g(B_{\perp} \neq 0, B_{\parallel}) \rangle$ . In both main figure and insets, dashed curves are fits to RMT, solid curves (labeled RMT+FJ) are fits to RMT including orbital coupling of  $B_{\parallel}$ , see text.

duce the low-temperature WL feature and therefore contribute to the saturation of WL observed in Ref. [19].

For both the high and low density material (respectively with AL and WL),  $\text{var } g$  at  $B_{\parallel} = 0$  is reduced upon application of a TRS-breaking perpendicular field, as seen in Figs. 1 and 2. This effect has been investigated previously for the weak SO (WL) case [18, 20], and has been observed but not analyzed for the strong SO (AL) case [4]. The solid theory curves in Figs. 1, 2 include thermal smearing and decoherence effects and use parameters obtained from fits of RMT to  $\langle g(B_{\perp}) \rangle$ , plus one additional parameter,  $f_{\text{var}}$ , (Table 1) to normalize the  $\text{var } g(B_{\perp} \neq 0)$  the RMT value. This factor compensates the assumption of multimode leads,  $N \gg 1$ , in the RMT [1], whereas the experiment has  $N = 2$ . RMT for  $\text{var } g$  in the case  $N = 2$  case has been given, but does not include SO or Zeeman terms [21].

We next investigate the effect of an in-plane magnetic field on  $\text{var } g$ , focusing first on the case where TRS is broken by a small perpendicular field,  $B_{\perp} \neq 0$ . As seen in Figs. 3 and 4,  $\text{var } g(B_{\perp} \neq 0, B_{\parallel})$  decreases with increasing  $B_{\parallel}$ , and saturates at large  $B_{\parallel}$ , giving reduction factors  $R = \text{var } g(B_{\perp} \neq 0, B_{\parallel} = 0) / \text{var } g(B_{\perp} \neq 0, B_{\parallel} \gg 0)$  between  $R \sim 1.6$  for the large high-density dots (which show AL at  $B_{\parallel} = 0$ ) and  $R \sim 4$  for large low-density dots

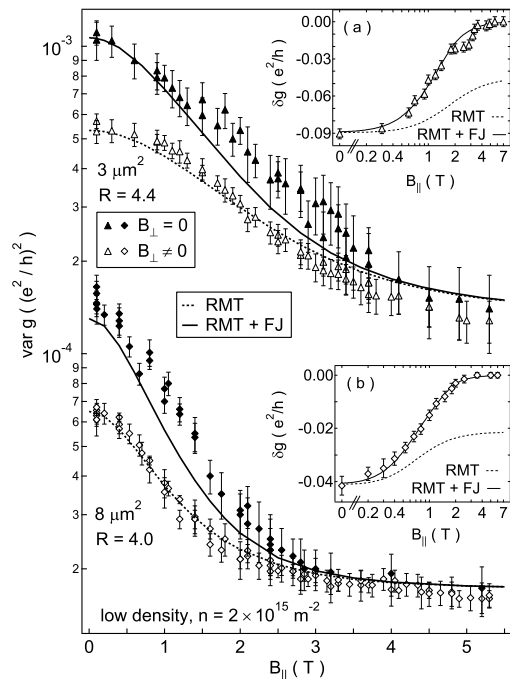


FIG. 4: As in Fig. 3, but for low density dots. In this case, the larger dot has a *larger* reduction factor in parallel field, consistent with RMT (curves). Orbital coupling of  $B_{\parallel}$  breaks TRS, making  $\text{var } g$  independent of  $B_{\perp}$  and quenching the quantum correction to average conductance,  $\delta g \rightarrow 0$ , (insets) on the same (dot-size-dependent) scale of  $B_{\parallel}$

(which show WL at  $B_{\parallel} = 0$ ). This range of values for  $R$  can be readily interpreted within RMT: For the large high density dots (relatively strong SO coupling, not suppressed by confinement), Kramers degeneracy is broken whenever TRS is broken, and there is weak spin mixing ( $\beta = 2, s = 1, 1 < \Sigma < 2$ ) at  $B_{\parallel} = 0$ . The effect of  $B_{\parallel}$  is to fully mix the Kramers pair ( $\beta = 2, s = 1, \Sigma = 1$ ), thus the reduction  $1 \leq R \leq 2$ . On the other hand, dots showing WL at  $B_{\parallel} = 0$  retain spin degeneracy ( $\beta = 2, s = 2, \Sigma = 2$ ) at  $B_{\parallel} = 0$ , which is then lifted by Zeeman coupling ( $\beta = 2, s = 1, \Sigma = 2$ ) and at larger  $B_{\parallel}$  mixed ( $\beta = 2, s = 1, \Sigma = 1$ ) due to SO coupling revived by  $B_{\parallel}$ , giving  $R \sim 4$ .

Spin mixing induced by  $B_{\parallel}$ , marking the  $\Sigma = 1$  to 2 crossover, occurs when a field-dependent energy scale  $\epsilon_{\perp}^Z$  exceeds the level broadening  $\tilde{\gamma} = \hbar(\tau_{\text{esc}}^{-1} + \tau_{\varphi}^{-1})^{-1}$  ( $\tau_{\text{esc}}^{-1} = N\Delta/\hbar$  is the escape rate from the dot). This new energy scale depends on both Zeeman and SO coupling,  $\epsilon_{\perp}^Z = \xi^2 \epsilon_Z^2 / (2E_T)(A/\lambda_{so}^2)$  [1], where  $\epsilon_Z = g\mu_B B$  is the Zeeman splitting,  $E_T$  is the Thouless energy (for ballistic dots  $E_T \sim \hbar v_F / \sqrt{A}$ , where  $v_F$  is the Fermi velocity), and  $\xi$  is a parameter of order one that depends on dot geometry as well as the direction of  $B_{\parallel}$  [1, 2]. Note that  $\epsilon_{\perp}^Z / \tilde{\gamma} \propto \epsilon_Z^2 A^{5/2}$  (when  $\tau_{\text{esc}} \ll \tau_{\varphi}$ ) so that the  $\Sigma = 1$  to 2 crossover field will depend on dot size. For the smallest dot, the crossover is inaccessible, and  $\Sigma = 1$  for all measured fields and  $R \sim 2$  due to breaking of Kramers degeneracy only

( $s = 2$  to  $1$ ). In the low density dots, the  $\Sigma = 1$  to  $2$  crossover is accessible, occurring around  $B_{\parallel} \sim 1(3)$  T for the larger (smaller) dot. The large high density dot has  $1 < \Sigma < 2$  already at  $B_{\parallel} = 0$  due to SO coupling, and the crossover to  $\Sigma = 2$  occurs around  $B_{\parallel} \sim 3$  T. Because of the undetermined coefficient  $\xi$ , the SO length  $\lambda_{so}$  cannot be independently extracted from  $\text{var } g(B_{\parallel})$ . Taking  $\xi$  as a single fit parameter, the dashed curves in Figs. 3 and 4 give the RMT results, which are in good agreement with experiment for all devices.

Finally, we investigate orbital effects of  $B_{\parallel}$  on  $\text{var } g$ , measured when TRS is not explicitly broken by a perpendicular field ( $B_{\perp} = 0$ ). Figures 3 and 4 show that as  $B_{\parallel}$  is increased,  $\text{var } g(B_{\perp} = 0, B_{\parallel})$  decreases sharply, approaching  $\text{var } g(B_{\perp} \neq 0, B_{\parallel})$ . At large  $B_{\parallel}$ ,  $\text{var } g$  becomes independent of  $B_{\perp}$  whereas RMT gives  $\text{var } g_{RMT}(B_{\perp} = 0)/\text{var } g_{RMT}(B_{\perp} \neq 0) = 2$  for all  $B_{\parallel}$ . On a similar scale of  $B_{\parallel}$ , WL corrections  $\delta g(B_{\parallel}) = \langle g(B_{\perp} = 0, B_{\parallel}) \rangle - \langle g(B_{\perp} \neq 0, B_{\parallel}) \rangle$  are also vanishing in all devices whereas RMT predicts a finite  $\delta g$ . As discussed previously [3, 4, 10], these effects result from the breaking of TRS by  $B_{\parallel}$  [8, 9].

Following Ref. [8] (FJ), we account for the suppression of  $\delta g(B_{\parallel})$  and  $\text{var } g(B_{\parallel})$  by introducing a field-dependent factor  $f_{FJ}(B_{\parallel}) = (1 + \tau_{B_{\parallel}}^{-1}/\tau_{esc}^{-1})^{-1}$ , where  $\tau_{B_{\parallel}}^{-1} \sim aB_{\parallel}^2 + bB_{\parallel}^6$ . The  $B_{\parallel}^2$  term reflects interface roughness and dopant inhomogeneities; the  $B_{\parallel}^6$  term is due to the asymmetry of the well. The RMT results

are then modified as  $\delta g(B_{\parallel}) = \delta g_{RMT}(B_{\parallel})f_{FJ}(B_{\parallel})$  and  $\text{var } g(B_{\perp} = 0, B_{\parallel}) = \text{var } g_{RMT}(B_{\perp} \neq 0, B_{\parallel})(1 + f_{FJ}(B_{\parallel}))$  to account for flux effects of the parallel field [22]. The coefficient  $a$  is obtained from a fit to the experimental  $\delta g(B_{\parallel})$  while  $b$  is estimated from device simulations [22] (Table I). The resulting theory curves for both  $\delta g(B_{\parallel})$  (solid curves, insets Figs. 3 and 4) and  $\text{var } g(B_{\perp} = 0, B_{\parallel})$  (solid curves, main panels) are in good agreement with experiment. We emphasize that the theoretical variance curves  $\text{var } g(B_{\perp} = 0, B_{\parallel})$  are not fit. Estimates of  $a, b$  based on correlation functions of parallel-field conductance fluctuations [10] are consistent with the values obtained here based on  $\delta g(B_{\parallel})$ .

In summary, mesoscopic conductance fluctuations in open quantum dots in presence of SO coupling and in-plane fields can be understood in terms of fundamental symmetries in the system, including novel partially broken spin rotation symmetries as well as time reversal symmetry, which can be broken by both perpendicular and in-plane fields.

We thank I. Aleiner, B. Altshuler, P. Brouwer, J. Creemers, V. Fal'ko, J. Folk, B. Halperin, T. Jungwirth and Y. Lyanda-Geller. This work was supported in part by DARPA-QuIST, DARPA-SpinS, ARO-MURI and NSF-NSEC. We also acknowledge support from NDSEG (J.B.M.) and the Harvard Society of Fellows (D.G.-G). Work at UCSB was supported by QUEST, an NSF Science and Technology Center.

- 
- [1] I. L. Aleiner *et al.*, Phys. Rev. Lett. **87**, 256801 (2001); J. N. H. J. Creemers *et al.*, Phys. Rev. B **68**, 125329 (2003).
- [2] B. I. Halperin *et al.*, Phys. Rev. Lett. **86**, 2106 (2001).
- [3] J. A. Folk *et al.*, Phys. Rev. Lett. **86**, 2102 (2001).
- [4] D. M. Zumbühl *et al.*, Phys. Rev. Lett. **89**, 276803 (2002).
- [5] A. V. Khaetskii *et al.*, Phys. Rev. B **61**, 12639 (2000); Y. V. Nazarov, Phys. Rev. B **64**, 2001 (2001).
- [6] T. Fujisawa *et al.*, Nature **419**, 278 (2002); J. M. Elzerman *et al.*, Nature **430**, 431 (2004); V. Golovach *et al.*, Phys. Rev. Lett. **93**, 16601 (2004).
- [7] P. W. Brouwer, *et al.*, Phys. Rev. B **65**, R81302 (2002).
- [8] V. I. Fal'ko *et al.*, Phys. Rev. B **65**, 81306 (2002).
- [9] J. S. Meyer, *et al.* Phys. Rev. Lett. **89**, 206601 (2002).
- [10] D. M. Zumbühl *et al.*, Phys. Rev. B **69**, 121305R (2004).
- [11] A. G. Mal'shukov *et al.*, Phys. Rev. B **56**, 6436 (1997); G. M. Minkov *et al.*, Phys. Rev. B **70**, 155323 (2004).
- [12] F. E. Meijer *et al.*, Phys. Rev. B **70**, 201307R (2004); F. E. Meijer *et al.*, cond-mat/0412731 (2004).
- [13] Y. Meir *et al.*, Phys. Rev. Lett. **63**, 798 (1989).
- [14] Y. B. Lyanda-Geller *et al.*, Phys. Rev. Lett. **72**, 1894 (1994).
- [15] B. L. Al'tshuler, JETP Lett. **41**, 648 (1985); B. L. Al'tshuler *et al.*, Sov. Phys. JETP **64**, 127 (1986); S. Feng, Phys. Rev. B **39**, 8722 (1989); A. D. Stone, Phys. Rev. B **39**, 10736 (1989); C. W. J. Beenakker, Rev. Mod. Phys. **69**, 731 (1997).
- [16] N. O. Birge *et al.*, Phys. Rev. Lett. **62**, 195 (1989); P. Debray *et al.*, Phys. Rev. Lett. **63**, 2264 (1989); O. Millo *et al.*, Phys. Rev. Lett. **65**, 1494 (1990); Y. K. Fukai *et al.*, Solid State Comm. **94**, 757 (1995); J. S. Moon *et al.*, Phys. Rev. B **56**, 15124 (1997).
- [17] B. Hackens *et al.*, Physica E **12**, 833 (2002). C. Gustin *et al.*, Physica E **17**, 154 (2003a).
- [18] I. H. Chan *et al.*, Phys. Rev. Lett. **74**, 3876 (1995).
- [19] A. G. Huibers *et al.*, Phys. Rev. Lett. **81**, 200 (1998); **83**, 5090 (1999).
- [20] A. G. Huibers *et al.*, Phys. Rev. Lett. **81**, 1917 (1998).
- [21] E. R. P. Alves *et al.*, Phys. Rev. Lett. **88**, 256805 (2002).
- [22] V. Fal'ko and T. Jungwirth, (private communication).